Thermal visco-elastic simulation model for tapering of laser-heated fused silica fiber

David R. Fairbanks

Charles Stark Draper Laboratory, Technical Staff
555 Technology Square, Cambridge, Massachusetts 02139

ABSTRACT

A computer simulation model represents the processes of heating a fused silica fiber and drawing it to form a taper. The model is a transient thermal and visco-elastic representation of an axial string of nodes that respond to laser heating and drawing in vacuum chucks. Preliminary sample simulation results are shown.

1. INTRODUCTION

This computer simulation model is intended as an aid in establishing optimal parameters for tapering single fibers, for eventual use in low-loss couplers. Early effort modeled the transient heating of fiber, by carbon-dioxide laser, as an axial string of nodes. Later, the visco-elastic drawing process using vacuum chucks was combined with the thermal model. Only the simulation model is discussed, as physical laboratory processing is not yet fully operational.

2. FIBER HEATING CONSIDERATIONS

The fiber heat source is a carbon-dioxide laser of 10.6–μm wavelength, and may be programmed to supply a time profile of continuous-wave power up to 25-watt limit. The beam passes through optics to align the beam and to create an elliptical Gaussian distribution. Optics may be chosen to achieve a variety of distributions. Mode field diameters (MFD) are defined as the major and minor axis width and height of the ellipse where the intensity drops to the $1/e^2$ point relative to the central maximum.

An important parameter is the fiber absorption efficiency. Bar-Ziv, et. al[1] have studied the heating of small spherical particles by carbon-dioxide laser beam. In the Mie regime the solutions for the heat distribution are cumbersome. However, total heat within the particle was solved and parametrically correlated. Fig. 1 shows fiber absorption efficiency versus diameter for a material with refractive index of 1.5, i.e., glass. The dimensionless particle size, $\alpha = \pi D/\lambda$, is for diameter D and wavelength λ. An additional scale has been added to relate fiber diameter for the 10.6-μm wavelength of illumination. McLachlan, et. al[2] has measured the extinction coefficient, k, for fused silica as about 0.20 at 1800°C to 0.15 at 1300°C. The figure indicates for this k value range the absorption efficiency is near unity and has minor sensitivity to size for diameters above 10 μm. While we have found no direct theoretical data for fibers, experimental measurements of fiber temperature under known laser heating conditions may lead to direct correlations of absorption efficiency with fiber temperature and diameter. Meanwhile, all results reported here are based on 100% absorption.

Calculations indicate that with unidirectional laser beam surface heating on one side only, temperature differences across the fiber diameter are quite small. For example, an 80-μm diameter fiber heated to 1800°C in a 25°C ambient would have a diametral temperture difference of about 4°C. From this it is concluded that knowledge of absorption distribution is not needed for diameters of this magnitude or less. Bi-directional illumination may be unnecessary, which greatly simplifies beam optics.

0-8194-0711-9/92/$4.00

Estimates were made of the total laser power required for heating a given fiber to the melting point. The following Table I shows the focused power delivery requirements in watts for a given set of elliptical Gaussian beam heights and widths. Assumptions include a single fiber, 80-μm fiber diameter, perfect alignment, and 100% absorption, to reach a maximum temperature of 1800°C.

This data is useful for selecting the lenses required for heating a given area of fiber. Two limitations to bear in mind are the maximum power available from the laser, and maximum beam diameter that can be obtained without diffraction, which is limited by the size of the lenses chosen.

Table I

Major axis width MFD (cm)	Laser power (w) for minor axis height MFD (μm)				
	20	80	160	320	640
0.7	0.5	0.8	1.5	2.9	5.8
1.4	1.0	1.6	3.0	5.8	11.5
2.8	2.1	3.3	5.9	11.6	23
5.6	4.2	6.6	11.8	23	46
11.2	8.3	13.1	24	46	92

3. THERMAL MODEL

The basic nodal heat balance conditions are shown in Fig. 2. Any imbalance in the heat flow terms results in instantaneous transient heat storage, in accordance with the following discrete representation for node n:

$$Q_{stored} = Q_{laser} + Q_{cond,\,n-1} + Q_{cond\,n+1} + Q_{amb} \tag{1}$$

where Q is a rate of heat flow to, or storage at, the node. The specific form of these terms expressed in dimensions, properties and states are as follows:

$$Alc\left(\frac{dT}{d\theta}\right) = qDl + kA/l\,(T_{n-1} - T_n) + kA/l\,(T_{n+1} - T_n) + K1\,(T_{amb} - T_n) \tag{2}$$

where:

A = cross-sectional area
c = specific heat
D = diameter
k = thermal conductivity
K = ambient conductance per unit length
l = length
q = absorbed laser heat flux
T = temperature
θ = time

A database of temperature-dependent property data was defined, based on catalog information from Corning[3] and Durasil,[4] and from the Touloukian[5] thermophysical property volumes. Curve-fit functions were then defined and incorporated into the model. These consist of nodal capacitance functions (specific heat) and

axial nodal conductance functions (conductivity). The fiber conductivity function includes an internal radiation term, important at high temperatures. The conductances were also altered to reflect the geometry changes during pull. Capacitances were not altered for geometry since a node represents a fixed volume of material. Property data for the fused silica was only shown up to about 1200°C. The curve-fit functions therefore extrapolate to the 1800°C level, with uncertain accuracy. Air conductivity is also extrapolated above 1200°C.

Considerable detail was focused on the fiber exterior thermal conductances to ambient. Contrary to usual expectation at the high temperatures, radiation is a small component of heat transfer relative to the air boundary. This is because as high temperatures are reached the emissivity of the fused silica reduces (from 0.80 to 0.06),[5] while the small diameter of the fiber results in "natural convection" in the regime of very small Grashof numbers where static radial air conduction predominates out to distances of many diameters.[6] This effect, plus the high air conductivity at elevated temperatures,[5] results in high air conductances. The combined effects of both air conduction and radiation were calculated as a function of both surface temperature and diameter. A least-squares fit expression was incorporated into the program to represent these effects on the nodal conductances to ambient. Nodal length change was also accounted for.

An important behavior resulting from these effects is that as the fiber diameter is reduced, under a fixed laser heat flux, the fiber cools off significantly. This is because the heat input varies directly with diameter, but the conductance to ambient is a weaker function of diameter. At the small diameters, the thermal capacitance of the air close to the fiber contributes a surprisingly large amount to the effective capacitance of the fiber; this effect is included in the model.

For determination of fiber viscosity, an additional temperature increment is estimated, based on uniform laser heat distribution through cross-section, and added to the surface temperature to produce a mean fiber temperature.

4. VISCO-ELASTIC MODEL

Assuming that fiber diameter changes gradually with length, the mechanical behavior was treated as a uni-axial load on a cylinder, for each node. The general case for time rate of strain under varying load and temperature includes three strain rate terms: elastic due to load, viscous due to load and viscosity (temperature), and expansion due to temperature. The evaluation of these terms for this problem, over the temperature range of interest for drawing fiber, shows that the elastic term is less than 0.2% of the viscous term, and the expansion term is even smaller. Both were neglected, with only the viscous term used. Jastrzebski[7] shows that the uni-axial loading strain rate with respect to time is

$$\frac{d\varepsilon}{d\theta} = \sigma/3\eta \qquad (3)$$

where ε is strain, θ is time, σ is tensile stress, and η is viscosity. Equation (3) is used in the model.

Data was supplied by Corning[8] on viscosity versus temperature for Corning #7940 silica. The data covers the temperature range of 1060°C to 1860°C, or viscosities from $10^{13.2}$ to 10^{6} poise. The model fit of this data is used over the whole temperature range down to 25°C, but with the value limited to avoid computer overflow.

5. COMBINED TAPER SIMULATION MODEL

A special-purpose Fortran program was developed to simulate both the transient thermal response and the viscous pull geometry changes during taper formation. This program incorporates a combination of explicit

forward estimation for property value changes, plus special implicit calculations. Two levels of implicit (backward) iterative schemes are used for solution at each time step. The inner level solves for temperatures and geometries, for a particular draw tensile force. The outer level adjusts tensile force to match the imposed chuck boundary velocity function, or to a force at which the fiber slips in the chucks. Each of these implicit loops meet convergence tests in about two iterations. Although nodal time-constants reach values as low as about 2 milliseconds, a simulation time-step of 250 milliseconds is satisfactory.

The basic nodal and boundary conditions are shown in Fig. 2. An initial node spacing of 0.10 cm was chosen as a compromise between accuracy and computation time. A total of 38 nodes represent the initial spacing from center line of symmetry to the edge of the chuck (at 25°C). Timeline functions are explicitly written for the laser heating maximum flux, and for the chuck velocity. All laser Gaussian flux distributions are scaled to the timeline function. Computer plotting routines have been added to the program.

The program currently treats the fiber as being a homogeneous cross-section of pure fused silica. It is expected that the viscosities of doped silica core and stress rods are significantly lower than that of pure silica cladding. It is intended that these considerations be accounted for in the stress determinations in future simulations, when specific data is found for the viscosities of the doped silica.

The property functions actually used in the simulation model are as shown in Table II.

Table II. Simulation Property Function Models

Ambient conductance per unit length (K = cal/s-cm-K, T = °C, D = cm) $K = 0.0001094 + 0.00757\ D - 2.588 \times 10^{-8}/D + 8.230 \times 10^{-8}\ T - 0.00519/T$
Fiber Conductivity (k = cal/s-cm-K, T = °C) $k = 0.00334 - 3.893 \times 10^{-7}\ T + 3.904 \times 10^{-12}\ (T+273)^3$
Fiber Specific Heat (c = cal/g-K, T = °C) $c = 0.1720 + 4.772 \times 10^{-5}\ T + 1.527 \times 10^{-3}\sqrt{T}$
Fiber Viscosity (η = poise = dyne-s/cm^2, T = °C) $\log(\eta) = -7.2758 + 2.7544 \times 10^4/(T + 273)$

6. PRELIMINARY THERMAL RESULTS

Prior to the definition of the visco-elastic taper portion of the model, some exploratory thermal simulations were done for constant fiber diameter. These are reported here.

Fig. 3 show fiber warmup for a uniform beam of 0.5-cm width from centerline. The fiber chucks, which are heat sinks at room temperature, are 2 centimeters apart. The fiber heats up rapidly with a uniform heat zone.

Other simulations (not shown) reveal that the axial conduction of the fiber is not sufficient to smooth out temperature variations caused by non-uniform axial heat flux, unless the spatial wavelengths are very small relative to the 0.5-cm length in Fig. 3. Axial non-uniformity of laser flux would thus likely show up as a temperature profile image, and a lumpy taper. Transient changes in heat flux were found to have a temperature step-response time-constant of about 80 milliseconds, for the 80-μm fiber near 1800°C.

Fig. 4 is another plot of temperature versus length and time, for a Gaussian beam distribution with major axis MFD of 1.4 cm. Fig. 5 shows the temperature distributions for various Gaussian width laser beams, in the hot zone. These simulations are helpful for choice of MFD values for the full taper simulations.

7. TAPER SIMULATION RESULTS

Two sample simulations are presented here. Both are for 80-μm fiber, and both have force applied without limitation due to chuck slippage. They also both apply the same constant chuck velocity, starting after one second of heating. Both have the same Gaussian heating MFD.

The first simulation is for a heating flux distribution that is constant with respect to time. Results are shown in Fig. 6,7 and 8. The taper geometry profiles of Fig. 6 appear to have a good shape, resulting in 47-μm minimum diameter and 1.3-cm draw length. Fig. 7, the temperature distribution of the same taper, shows that the fiber cools with time due to reductions of diameter and axial movement. This causes the pull forces and stresses to increase, as shown in Fig. 8.

The second simulation is for a heating flux distribution which has the same values at 1 second as in the first simulation, but then has the values increase with a time ramp. These results are shown in Fig. 9, 10 and 11. The taper shapes of Fig. 9 are similar to those of Fig. 6, but the simulation was run for a longer time, resulting in 28-μm minimum diameter and 2.8-cm draw length. Fig. 10 shows that the heat ramp results in a reduced fiber cooling rate. Fig. 11 shows much reduced forces and stresses relative to Fig. 8.

These two example simulations were run to demonstrate the computer program and simulation models.

8. CONCLUSIONS

A computer simulation model has been developed and demonstrated. It has the potential to aid in the selection of processing parameters for achieving optimal fiber taper shapes. Many different parameters may be parametrically varied for simulations. While only sample demonstration results are shown, work is progressing with the laboratory processing station, so that the simulation program may be checked against actual tapers and adjusted as needed. The simulation model should then be a useful adjunct to the processing station.

9. ACKNOWLEDGMENTS

This computer simulation model development was supported by internal funding at the Charles Stark Draper Laboratory, as part of a development task under the direction of R. Dahlgren.

10. REFERENCES

1. E. Bar-Ziv and A. F. Sarofim, "The Electrodynamic Chamber: A Tool for Studying High Temperature Kinetics Involving Liquid and Solid Particles", Progress in Energy and Combustion Science, 1991, Vol. 17, p.31.

2. A. D. McLachlan and F. P. Meyer, "Temperature Dependence of the Extinction Coefficient of Fused Silica for CO_2 Laser Wavelengths", Applied Optics, Vol. 26, No. 9, 1 May 1987.

3. Fused Silica, Catalog, Corning Inc., Corning, NY.

4. Synthetic Fused Silica, Catalog 302-M, Dynasil Corp. of America, Berlin, NJ.

5. Y.S. Touloukian and C.Y. Ho, "Thermophysical Properties of Matter", The TPRC Data Series, Purdue University, various volumes, IFI Plenum Publishing Campany, New York, 1979.

6. F. Kreith, *Principles of Heat Transfer*, p. 305 (Scranton, PA: International Text Book Co., 1963).

7. Z.D. Jastrzebski, *Nature of Properties of Engineering Materials*, pp. 185-188 (John Wiley & Sons, 1964).

8. P. Schermerhorn, Fused Silica Viscosity Data (personal communication), Corning Inc., Corning, NY.

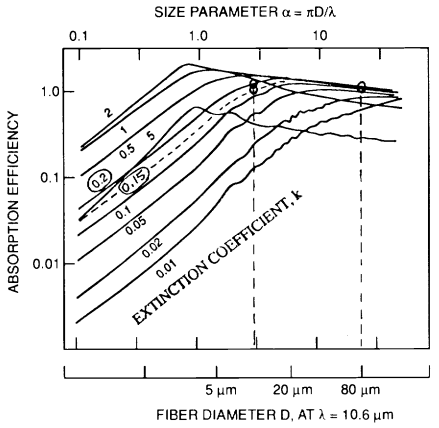

Fig. 1. The absorption efficiency as a function of the size parameters α for n = 1.5 and various values of the extinction coefficient k. Reprinted with permission.[1]

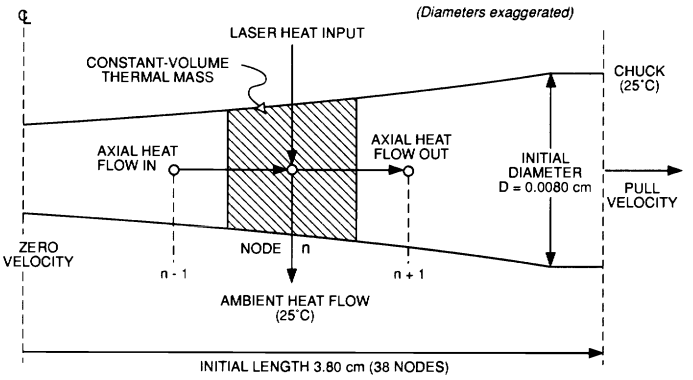

Fig. 2. Simulation model basic nodal and boundary conditions.

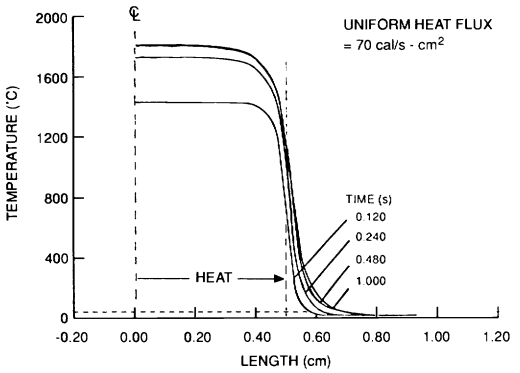

Fig. 3. Temperature of 80-μm fiber for uniform 1.0-cm heating.

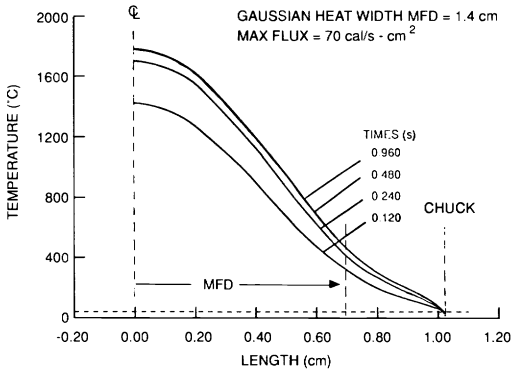

Fig. 4. Temperature profiles for 80-μm fiber, for 1.4-cm Gaussian heating width MFD.

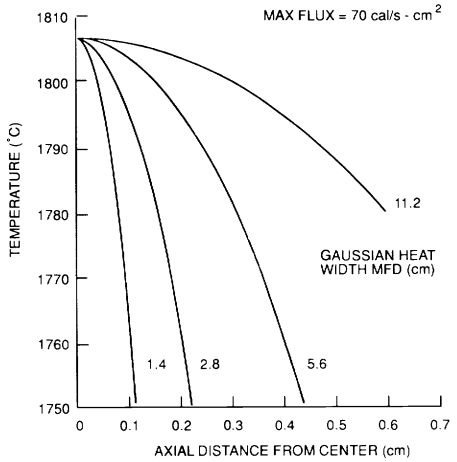

Fig. 5. Fiber temperature vs Gaussian heat width along 80-μm fiber, at 0.96 s.

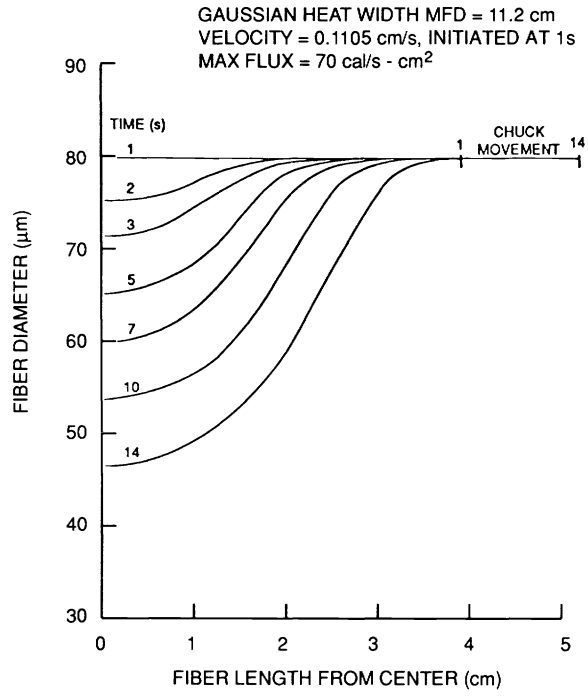

Fig. 6. Fiber taper geometry vs time with heat input constant with time.

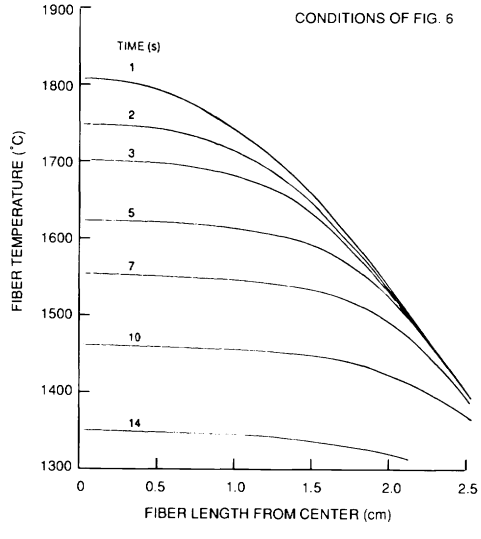

Fig. 7. Fiber taper temperature vs time, for the simulation of Fig. 6.

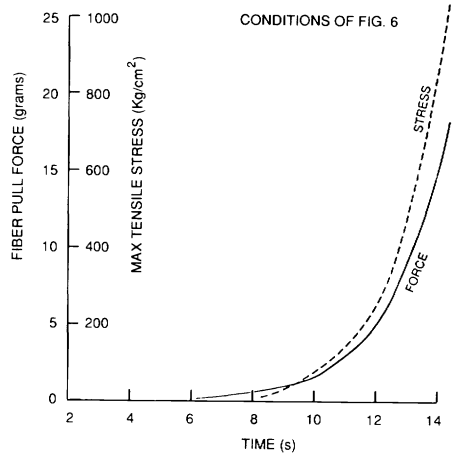

Fig. 8. Fiber taper force and stress vs time, for the simulation of Fig. 6.

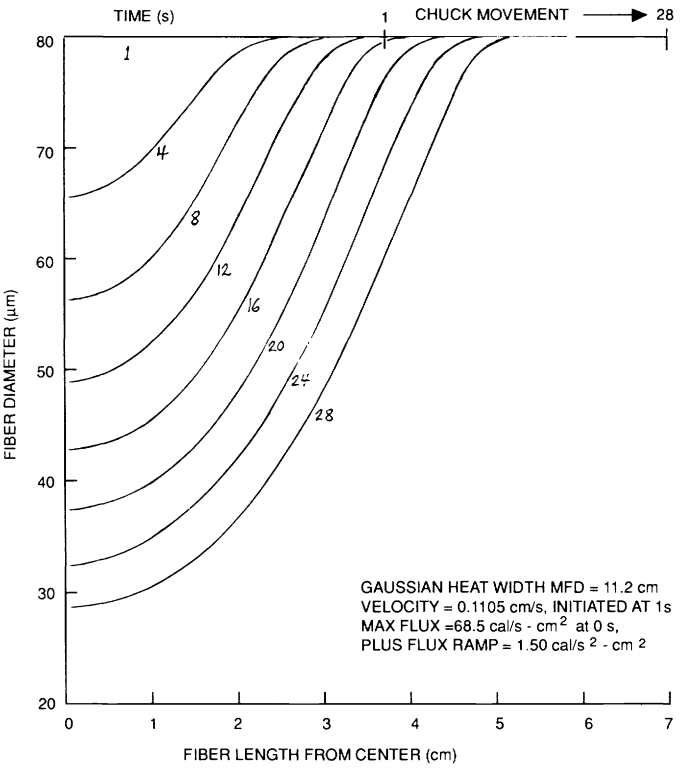

Fig. 9. Fiber taper geometry vs time, for heat input ramped with time.

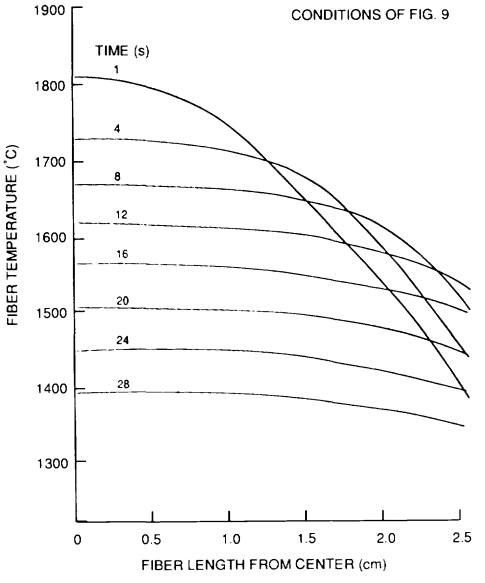

Fig. 10. Fiber taper temperature vs time, for the simulation of Fig. 9.

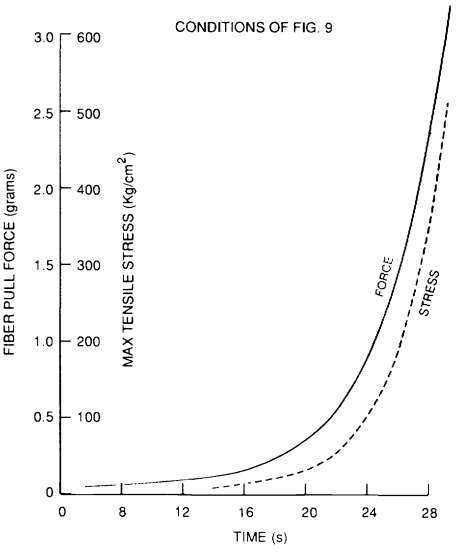

Fig. 11. Fiber taper force and stress vs time, for the simulation of Fig. 9.